# ChemComm

Accepted Manuscript


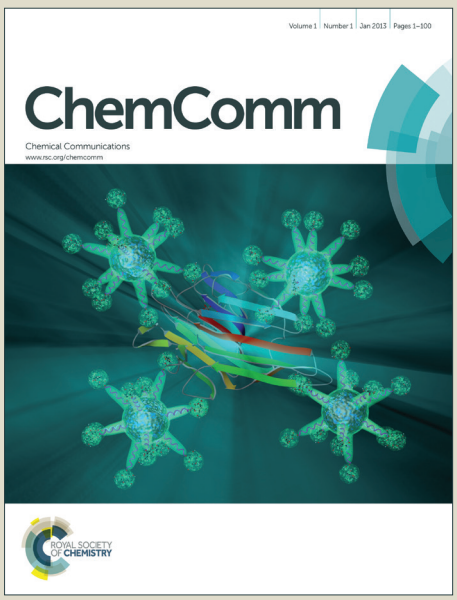





ROYAL SOCIETY OF CHEMISTRY

www.rsc.org/chemcomm

Cite this: DOI: 10.1039/c0xx00000x

www.rsc.org/xxxxxx

ARTICLE TYPE

# Hybrid polymer micelles capable of cRGD targeting and pH-triggered surface charge conversion for tumor selective accumulation and promoted uptake

**Xiuli Hu,[a] Xingang Guan,[a,b] Jing Li,[a] Qing Pei,[a,c] Ming Liu,[a,c] Zhigang Xie,*[a] Xiabin Jing[a]**

***Received (in XXX, XXX) XthXXXXXXXXX 20XX, Accepted Xth XXXXXXXXX 20XX***
**DOI: 10.1039/b000000x**

**This study presents both tumor-targeting ligands (cRGD)) and pH-activated surface charge-conversional moiety (imidazole) decorated micelles for Dox delivery. cRGD is expected to induce preferential tumor accumulation, while imidazole switches on positive charge in tumor acid environment, which leads to enhanced micelle uptake by tumor cells.**

Doxorubicin (Dox) is a widely used anticancer drug in the treatment of many types of cancers. However, systemic administration of Dox itself elicits severe cardiac toxicity due to the lack of ability to target cancer cells.[1] To improve the therapeutic efficacy of Dox, various drug delivery systems have been reported. Among which, polymeric micelles assembled from block copolymers offer an opportunity to alter the pharmacokinetic profile of drugs, to reduce systemic toxicity, and to improve the therapeutic index.[2]

Recently, the tumor microenvironments have attracted special attention and have been utilized to design responsive delivery system. For example, the tumor extracellular environment is more acidic (pH 6.0–6.5) than blood (pH~7.4), and the pH values of endosomes and lysosomes are even lower (pH 5.0–5.5).[3] Hypoxia is also observed in solid tumors and affects the therapy of anticancer drugs.[4] Zhou and his workers reported pH-sensitive Dox prodrug micelles with folic acid as targeting moiety.[5] Hypoxia- and pH-sensitive nanoparticles have been designed and evaluated based on the tumor microenvironment.[6] It has been reported by many researchers that positively charged nanoparticles show higher affinity for negatively charged cell membranes and thus can be readily internalized by the cells.[3b, 7] Further, in order to avoid compromising their blood circulation time caused by the strong interaction of positive charge with serum components, charge-conversion have been used and proved to be an efficient method.[7] However, most of the present studies ignore that the pre-condition is to ensure the preferential accumulation of nanoparticles in tumor region. Only passive targeting to tumor by enhanced permeability and retention (EPR) effect is limited. Better targeting capability should be achieved by modification with suitable active-targeting ligands.

Active targeting is usually achieved by chemically attaching a targeting ligand onto the micelles that strongly interacts with antigen or receptor existing on the target organ, tissue, or cells.[8] RGD sequence has been identified selectively binding to $\alpha_v\beta_3$ and $\alpha_v\beta_5$ integrins which are overexpressed in tumor vascular endothelial cells and some solid tumors.[9] Ruoslahti et al. observed enhanced tumor-specific delivery of different compounds including small molecule (Dox), nanoparticles (paclitaxel and doxorubicin liposomes), and monoclonal antibody (trastuzumab).[10] Kataoka et al. achieved highly efficient drug delivery to glioblastoma by using a platinum anticancer drug-incorporating polymeric micelle with cyclic RGD (c(RGDfK), cyclic Arginine-Glycine-(Aspartic acid)-(D-Tyrosine)-Lysine) ligand molecules.[11]

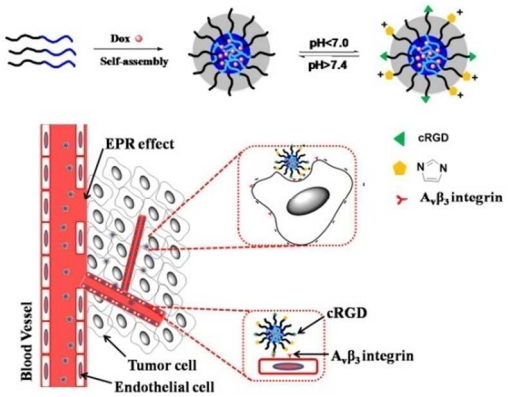


**Scheme 1**. Assembly, RGD targeting and pH-activated surface charge-conversion of the micelles.

In the present work, we designed and synthesized dual functional micelles combining active targeting and tumor microenvironment stimuli response, which have been rarely investigated. The cyclic RGD peptide c(RGDfK) was selected as an active targeting moiety. Imidazole (pKa=~6.8) was selected as the charge-conversional group because of its protonation in tumor microenvironment. Moreover, the transformation of protonation-deprotonation is rapid and reversible.[12] cRGD and imidazole decorated PEG-b-PLA copolymers were used to obtain functional micelles by co-assembly method. Once the micelles were accumulated at the tumor site through RGD mediated active targeting, the surface imidazole groups were activated to be positively charged in response to the pH value outside of tumor

blood vessel (pH<7) and accordingly cellular internalization should be enhanced (Scheme 1).

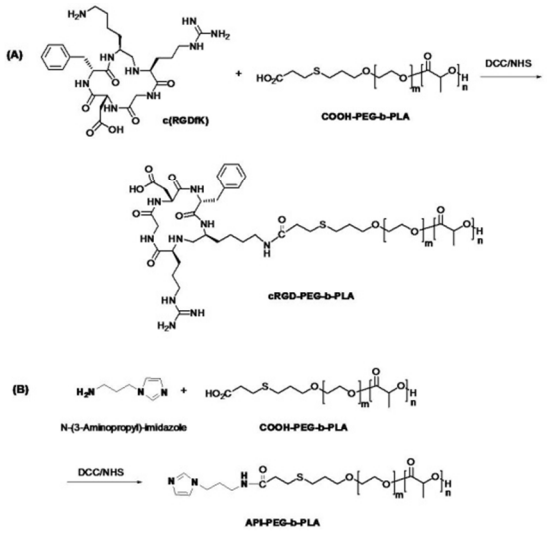


**Figure 1**. Synthetic routes of (A) cRGD-PEG-b-PLA and (B) API-PEG-b-PLA.

First, PEG terminal functionalized copolymer HOOC-PEG-b-PLA was prepared using radical-mediated thiol-ene reaction between the allyl group and 3-mercaptopropionic acid (MPA) reported elsewhere,[13] and its chemical structure was characterized by $^1$H NMR (Figure S1, see ESI). This amphiphilic compolymer could self-assemble into micelles in aqueous solution and the critical micelle concentration (CMC) was detected to be $3.3\times10^{-3}$ g/L (Figure S2, see ESI). cRGD and imidazole decorated copolymers were prepared by reacting c(RGDfK) and N-(3-aminopropyl)-imidazole (API) in the presence of DCC and NHS, respectively. The synthetic route was shown in Figure 1.

Attachment of c(RGDfK) peptide onto HOOC-PEG-b-PLA was confirmed by fluorimetric assay, in which 9,10-phenanthrenequinone was reacted with the arginine residue in c(RGDfK) to generate a specific fluorescent compound. By fluorescence measurement of this compound ($\lambda_{ex}$=312 nm, $\lambda_{em}$=340~570nm), the molar ratio of cRGD peptide to polymer was determined to be 1:2.17, i.e., averagely 46% of HOOC-PEG-b-PLA was labeled with c(RGDfK). N-(3-aminopropyl)-imidazole (API) was conjugated onto HOOC-PEG-b-PLA by the similar method and the structure of API-PEG-b-PLA was confirmed by $^1$H NMR spectroscopy (Figure S3, see ESI).

For targeting therapy, the co-assembly method has been proven to be a good choice, for it is easier and more convenient to tailor the content of targeting moiety in the micelles. So in this study, three copolymers including mPEG-b-PLA, c(RGDfK)-PEG-b-PLA and API-PEG-b-PLA with the similar polymerization degree were synthesized and used to adjust the content of cRGD and API in the micelles. cRGD and/or imidazole decorated micelles were prepared similarly by using desired ratios of c(RGDfK)-PEG-b-PLA, API-PEG-b-PLA, and mPEG-b-PLA as the starting materials. Typically, two cRGD micelles were prepared by using a mixture of c(RGDfK)-PEG-b-PLA and mPEG-b-PLA with weight ratio of 10/90 and 20/80, respectively. The obtained Dox-loaded micelles were abbreviated as $RGD_{10}$-M(Dox) and $RGD_{20}$-M(Dox), respectively. Considering the RGD content in the copolymer of c(RGDfK)-PEG-b-PLA was 46%, the real RGD content in the micelles was calculated to be 4.6 and 9.2% in $RGD_{10}$-M(Dox) and $RGD_{20}$-M(Dox), respectively. Similarly, two kinds of different imidazole micelles were prepared by adjusting the ratio of API-PEG-b-PLA and mPEG-b-PLA:$API_{20}$-M(Dox), and $API_{50}$-M(Dox). Considering the cellular uptake observed in the following part, cRGD and imidazole dual targeted micelles RGD/API-M(Dox) were prepared by using a mixture of c(RGDfK)-PEG-b-PLA, API-PEG-b-PLA and mPEG-b-PLA in the ratio of 2:5:3. The drug content of feed for all the seven micelles listed in Table 1 was 10 wt% and the drug loading efficiency were almost 100%. The diameters of drug loaded micelles do not change very much for different ratio of polymers and are between 50–60 nm as shown in Table S1. The zeta potential of all micelles was around zero in water (Table S1, see ESI), which indicated that the micelles were neutral during blood circulation. The hybrid micelle exhibited a sustained-release profile and the adding of c(RGDfK)-PEG-b-PLA and API-PEG-b-PLA did not change the drug release very much (Figure S4, see ESI).

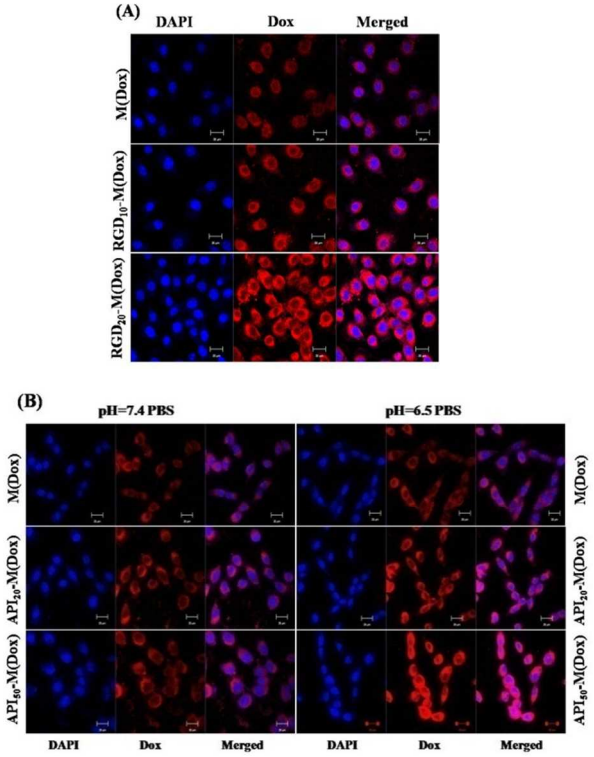


**Figure 2.** In vitro CLSM images of EMT6 cells treated with (A) M(Dox), $RGD_{10}$-M(Dox) and $RGD_{20}$-M(Dox) micelles at pH 7.4 PBS; (B) M(Dox), $API_{20}$-M(Dox) and $API_{50}$-M(Dox) micelles at pH 7.4 (left) and pH 6.5 (right) for 0.5 h at 37°C at Dox concentration of 10 μg/mL. Scale bars represent 20 μm in all images.

To evaluate the biological activities of the ligand-linked micelles, we analyzed their cellular uptake by virtue of the inherent fluorescence of Dox itself for the CLSM measurement. As shown in Figure 2(A), RGD modification significantly enhanced the cellular uptake by EMT6 cells. After treatment for only 0.5 h, the cellular uptake of $RGD_{10}$-M(Dox) was higher than that of M(Dox) and even more $RGD_{20}$-M(Dox) were uptaken. It is noticed that the fluorescence all came from the cytoplasm and

there was almost no fluorescence in the nucleus region, indicating that the drug-loaded micelles were endocytosed into the cells and no drug was released from the micelles in such a short time period. On the basis of the CLSM images, $RGD_{20}$-M(Dox) was chosen for the following cytotoxicity and biodistribution evaluation.

To investigate the influence of pH on the cellular uptake of the imidazole-decorated micelles, M(Dox), $API_{20}$-M(Dox) and $API_{50}$-M(Dox) micelles were incubated in EMT6 cells at different pH values (pH 6.5 and 7.4). As shown in Figure 2(B), greater uptakes of the micelles were observed for both $API_{20}$-M(Dox) and $API_{50}$-M(Dox) at pH 6.5 mimicking the tumor microenvironment than that at pH 7.4 mimicking the blood while M(Dox) micelles did not show so big difference. Semi-quantitatively, the Dox fluorescence intensity difference between pH 6.5 and 7.4 were in the order of M(Dox)<$API_{20}$-M(Dox)<$API_{50}$-M(Dox). Therefore, the enhanced micelle uptake by the cells was due to the presence of the imidazole groups or due to more protonation of them at pH 6.5 than at pH 7.4.

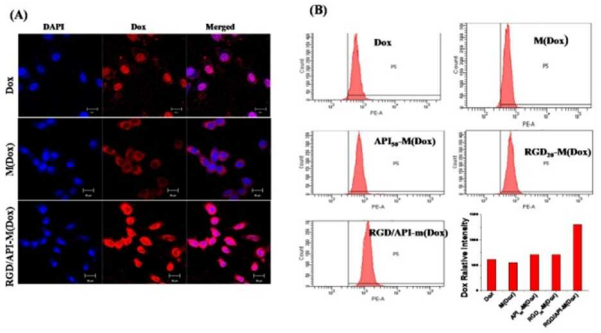


**Figure 3.** (A) In vitro CLSM images of EMT6 cells treated with Dox, M(Dox), and RGD/API-M(Dox) micellesfor 0.5 h at 37°C at pH 6.5. All pictures show the nuclei (blue), Dox (red) and merged images. Scale bars represent 20 μm in all images. (B) Flow cytometry quantification of cellular internalization of free Dox, M(Dox), $API_{20}$-M(Dox), $API_{50}$-M(Dox) and RGD/API-M(Dox) micellesfor 0.5 h at 37°C at pH 6.5.

Based on the above results, cRGD- and imidazole-decorated micelles were designed with the weight content of c(RGDfK)-PEG-b-PLA/API-PEG-b-PLA/ mPEG-b-PLA of 20/50/30. Figure 4 Shows the fluorescence images of EMT6 cells treated by Dox, M(Dox) and RGD/API-M(Dox) tested by CLSM and the fluorescence intensity diistributions of EMT6 cells treated by Dox, M(Dox), $API_{50}$-M(Dox), $RGD_{20}$-M(Dox) and RGD/API-M(Dox) tested by flow cytometry. As shown in Figure 3(A), compared with M(Dox) treated cells, RGD/API-M(Dox) treated cells showed more intense Dox fluorescenc in both cytoplasmic and nucleus area, in agreement with Figure 2 and free Dox was distributed mainly in the nuclei, indicating rapid internalization of free Dox by the cells via simple diffusion. The CLSM results in Figure 2 and 3(A) were supported by the flow cytometric analysis. As shown in Figure 3(B), the Dox intensity followed the order of pure Dox ≈ M(Dox) < $RGD_{20}$-M(Dox) ≈ $API_{50}$-M(Dox) < RGD/API-M(Dox). In short, the dual functional RGD/API-M(Dox) micelles had the fastest and greatest cellular uptake compared to other micelles.

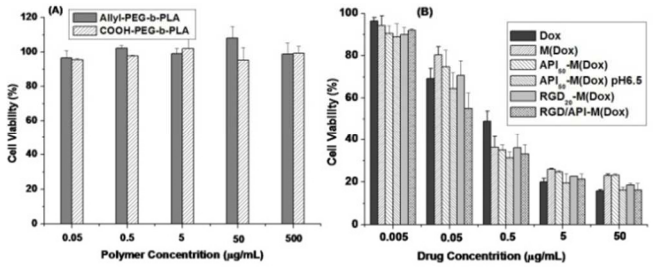


**Figure 4.** Viability of EMT6 cells treated with (A) blank micelles, (B) free Dox, M(Dox), $API_{50}$-M(Dox), $API_{50}$-M(Dox) at pH 6.5, $RGD_{20}$-M(Dox) and RGD/API-M(Dox) micelles after incubation 48 h at 37 °C. All the results were repeated three times, and presented as mean±SD.

The cytotoxicity of the blank micelles was evaluated. After EMT6 cells were incubated with allyl-PEG-b-PLA and HOOC-PEG-b-PLA micelles at various concentrations at 37 °C for 48 h, the cell viability was determined by the MTT assay (Figure 4A). Both of the two blank micelles showed very low cytotoxicity (>95% viability) at concentrations up to 500 mg $mL^{-1}$.The cytotoxicity of the Dox-loaded micelles was investigated with free Dox as a positive control and blank culture medium without drugs as a negative control. Figure 4B shows the cell viability after 48 h culture with various Dox formulations at various Dox concentrations. It can be seen that cytotoxicities of the tested formulations were all concentration dependent. Of the four Dox-loaded micelles, M(Dox) had the lowest cytotoxicity and RGD/API-M(Dox) micelles showed the highest cytotoxicity at all Dox concentrations. The imidazole-decorated $API_{50}$-M(Dox) micelles showed higher cytotoxicity at pH 6.5 than at pH 7.4.

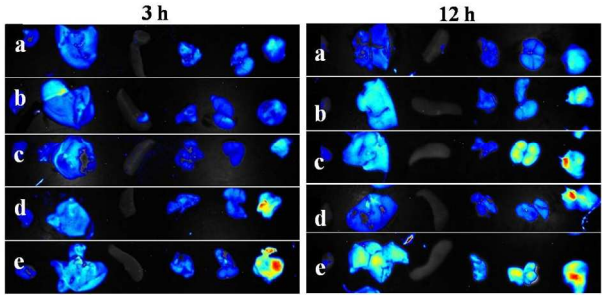


**Figure 5**. (A) Ex vivo Dox fluorescence images showing the drug bio-distribution of (a) free Dox, (b) M(Dox), (c) $API_{50}$-M(Dox), (d) $RGD_{20}$-M(Dox)and (e) RGD/API-M(Dox) in Balbc mice bearing EMT6 tumor at 3 and 12 h post-injection; (B) Average signals collected from the major organs (heart, liver, spleen, lung and kidney) and tumor in Balbc mice bearing EMT6tumor after the treatment of (a) free Dox, (b) M(Dox), (c) $API_{50}$-M(Dox), (d) $RGD_{20}$-M(Dox)and (e) RGD/API-M(Dox) at different time points.

The effect of RGD and imidazole groups on the in vivo distribution of micelles was further investigated. Figure 5 shows the Dox signals collected from isolated visceral organs (heart, liver, spleen, lung, kidney, and tumor) at 3 and 12 h post injection. We can obtain the following conclusions from Figure 6: (1) most drugs were accumulated in the liver and tumor and their contents in the lung and kidney were lower than that in the liver and tumor and were lowest in the heart and spleen; (2) the blood clearance of free Dox was faster than that of micelle formations because the Dox signals in various organs were lower than those of the micelles at both 3 and 12 h after injection; (3) More $API_{50}$-

M(Dox) and $RGD_{20}$-M(Dox) were observed in the tumor at 3 h and 12 h, whereas the strongest fluorescence intensity was observed for RGD/API-M(Dox)) micelles, indicating the targeting and synergistic effect of RGD and imidazole groups.

In summary, dual-functional Dox-loaded micelles modified with cRGD and imidazoles were successfully developed. The hydrodynamic diameters of the micelles were between 50-70 nm, and the drug encapsulation efficiency was almost 100% when the drug loading content was 10 wt%. The encapsulated drug exhibited a sustained-release profile. Enhanced uptake mediated by the binding of RGD to the $\alpha_v\beta_3$ integrin and surface charge conversion was observed by CLSM and flow cytometry. Biodistribution studies demonstrated preferential accumulation in the tumor tissue than non-decorated micelles. Our proof of concept in vitro and in vivo shows that this cRGD and imidazole dual-functional micelles have great advantages such as increasing tumor accumulation and intracellular uptake and represent an attractive approach to be optimizedand developed in the future.

This work was financially supported by the National Science Foundation of China (No. 51373167 and 91227118).

## Notes and references

[a] *State Key Laboratory of Polymer Physics and Chemistry, Changchun Institute of Applied Chemistry, Chinese Academy of Sciences, Changchun 130022, P. R. China. Fax: +86-431-85262779; Tel: +86-431-85262779; E-mail: xiez@ciac.ac.cn*

[b] *Life Science Research Center, Beihua University, Jilin 132013, P. R. China*

[c] *The University of Chinese Academy of Sciences, Beijing 100049, P. R. China*

† Electronic Supplementary Information (ESI) available: [details of any supplementary information available should be included here]. See DOI: 10.1039/b000000x/

‡ Footnotes should appear here. These might include comments relevant to but not central to the matter under discussion, limited experimental and spectral data, and crystallographic data.

1. (a) M. Hruby, C. Konak, K. Ulbrich, *J. Controlled Release* 2005**, 103** 137; (b) C. Carvalho, R. Santos, S. Cardoso, S. Correia, P. J. Oliveira, M. S. Santos, P. I. Moreira, *Curr. Med. Chem.* 2009**, 16**, 3267.

2. (a) X. Hu, X. Jing, *Expert Opin. Drug Del.* 2009**, 6**, 1079; (b) Z. Cheng, A. Al Zaki, J. Z. Hui, V. R. Muzykantov, A. Tsourkas, *Science* 2012**, 338**, 903; (c) P. Couvreur, *Adv. Drug Deliver. Rev.* 2013**, 65**, 21.

3. (a) M. Meyer, A. Philipp, R. Oskuee, C. Schmidt, E. Wagner, *J. Am. Chem. Soc.* 2008**, 130**, 3272; (b) J. Z. Du, T. M. Sun, W. J. Song, J. Wu, J. Wang, *Angew. Chem. Int. Ed.* 2010**, 49**, 3621; (c) Y. Lee, T. Ishii, H. Cabral, H. J. Kim, J. H. Seo, N. Nishiyama, H. Oshima, K. Osada, K. Kataoka, *Angew. Chem. Int. Ed.* 2009**, 48**, 5309.

4. (a) W. Piao, S. Tsuda, Y. Tanaka, S. Maeda, F. Y. Liu, S. Takahashi, Y. Kushida, T. Komatsu, T. Ueno, T. Terai, T. Nakazawa, M. Uchiyama, K. Morokuma, T. Nagano, K. Hanaoka, *Angew. Chem. Int. Ed.* 2013**, 52** (49), 13028-13032; (b) K. Okuda, Y. Okabe, T. Kadonosono, T. Ueno, B. G. M. Youssif, S. Kizaka-Kondoh, H. Nagasawa, *Bioconjugate Chem.* 2012**, 23**, 324.

5. X. Guo, C. Shi, J. Wang, S. Di, S. Zhou, *Biomaterials* 2013**, 34** (18), 4544-4554.

6. F. Perche, S. Biswas, T. Wang, L. Zhu, V. P. Torchilin, *Angew. Chem. Int. Ed.* 2014, **53** (13), 3362-3366.

7. (a) E. C. Cho, J. Xie, P. A. Wurm, Y. Xia, *Nano Letters* 2009**, 9**, 1080; (b) Y. Lee, K. Miyata, M. Oba, T. Ishii, S. Fukushima, M. Han, H. Koyama, N. Nishiyama, K. Kataoka, *Angew. Chem. Int. Ed.* 2008**, 47** (28), 5163-5166.

8. (a) X. H. Peng, Y. Wang, D. Huang, Y. Wang, H. J. Shin, Z. Chen, M. B. Spewak, H. Mao, X. Wang, Y. Wang, Z. Chen, S. Nie, D. M. Shin, *ACS nano* 2011**, 5**, 9480; (b) Y. Vachutinsky, M. Oba, K. Miyata, S. Hiki, M. R. Kano, N. Nishiyama, H. Koyama, K. Miyazono, K. Kataoka, *J. Controlled Release* 2011**, 149**, 51; (c) Y. Z. Du, L. L. Cai, P. Liu, J. You, H. Yuan, F. Q. Hu, *Biomaterials* 2012**, 33**, 8858; (d) V. A. Sethuraman, Y. H. Bae, *J. Controlled Release* 2007**, 118**, 216.

9. (a) F. Danhier, B. Vroman, N. Lecouturier, N. Crokart, V. Pourcelle, H. Freichels, C. Jerome, J. Marchand-Brynaert, O. Feron, V. Preat, *J. Controlled Release* 2009**, 140**, 166; (b) C. Zhan, B. Gu, C. Xie, L. Li, Y. Liu, W. Lu, *J. Controlled Release* 2010**, 143**, 136.

10. (a) K. N. Sugahara, T. Teesalu, P. P. Karmali, V. R. Kotamraju, L. Agemy,O. M. Girard, D. Hanahan, R. F. Mattrey, E. Ruoslahti, *Cancer Cell* 2009**, 16**, 510; (b) K. N. Sugahara, T. Teesalu, P. P. Karmali, V. R. Kotamraju, L. Agemy, D. R. Greenwald, E. Ruoslahti, *Science* 2010**, 328**, 1031.

11. Y. Miura, T. Takenaka, K. Toh, S. Wu, H. Nishihara, M. R. Kano, Y. Ino, T. Nomoto, Y. Matsumoto, H. Koyama, H. Cabral, N. Nishiyama, K. Kataoka, *ACS nano* 2013**, 7**, 8583.

12. C. S. Lee, W. Park, Y. U. Jo, K. Na, *Chem. commun.,* 2014**, 50**, 4354.

13. J. Yue, X. Li, G. Mo, R. Wang, Y. Huang, X. Jing, *Macromolecules* 2010**, 43**, 964.